A Synthetic Human Antibody Antagonizes IL-18Rβ Signaling Through an Allosteric Mechanism

Shusu Liu[1,†], **Shane Miersch**[2,†], **Ping Li**[1,3], **Bingxin Bai**[1], **Chunchun Liu**[1], **Wenming Qin**[4], **Jie Su**[1], **Haiming Huang**[2,5], **James Pan**[2], **Sachdev S. Sidhu**[1,2] and **Donghui Wu**[1]

1 - Laboratory of Antibody Engineering, Shanghai Institute for Advanced Immunochemical Studies, ShanghaiTech University, Shanghai, China

2 - Banting and Best Department of Medical Research, Terrence Donnelly Center for Cellular and Biomolecular Research, University of Toronto, Toronto, ON, Canada

3 - Institute of Biochemistry and Cell Biology, Shanghai Institutes for Biological Sciences, University of Chinese Academy of Sciences, China

4 - National Facility for Protein Science (Shanghai), Shanghai Advanced Research Institute (Zhangjiang Lab), Chinese Academy of Sciences, Shanghai, China

5 - Shanghai Asian United Antibody Medical Co., Shanghai, China

Correspondence to Donghui Wu and Sachdev S. Sidhu: Laboratory of Antibody Engineering, Shanghai Institute for Advanced Immunochemical Studies, ShanghaiTech University, Shanghai, China. sachdev.sidhu@utoronto.ca, wudh@-shanghaitech.edu.cn

Abstract

The interleukin-18 subfamily belongs to the interleukin-1 family and plays an important role in modulating innate and adaptive immune responses. Dysregulation of IL-18 has been implicated in or correlated with numerous diseases, including inflammatory diseases, autoimmune disorders, and cancer. Thus, blockade of IL-18 signaling may offer therapeutic benefits in many pathological settings. Here, we report the development of synthetic human antibodies that target human IL-18Rβ and block IL-18-mediated IFN-γ secretion by inhibiting NF-κB and MAPK dependent pathways. The crystal structure of a potent antagonist antibody in complex with IL-18Rβ revealed inhibition through an unexpected allosteric mechanism. Our findings offer a novel means for therapeutic intervention in the IL-18 pathway and may provide a new strategy for targeting cytokine receptors.

Introduction

The interleukin-1 (IL-1) family is one of the largest cytokine families, with members playing critical roles in regulating innate and acquired immunity [1]. The family contains 11 members, grouped into IL-1, IL-18, and IL-36 subfamilies [1]. IL-18 is a particularly important family member, which acts as a pro-inflammatory cytokine that modulates diverse immune cell populations to shape an intertwined network of immune responses [2−6]. Consequently, dysregulation of IL-18 has been implicated in or correlated with numerous diseases, including systemic lupus erythematosus (SLE), rheumatoid arthritis (RA), psoriasis, Crohn's disease (CD), metabolic syndrome, cardiovascular diseases, lung inflammatory diseases, hemophagocytic syndromes, systemic juvenile idiopathic arthritis, sepsis, and cancer [2,7]. Thus, blockade of IL-18 signaling may offer therapeutic benefits in many pathological settings.

IL-18 is produced as an inactive precursor and becomes an active cytokine upon caspase-1 cleavage [8]. Upon secretion, bioactive IL-18 can stimulate target cells in a stepwise manner by binding to IL-18 receptor-α (IL-18Rα) to form a binary complex that then recruits an accessory protein IL-18 receptor-β (IL-18Rβ) to form a high-

affinity ternary complex, which triggers downstream signaling [9]. Formation of the ternary-complex positions the intracellular Toll-IL-1 receptor (TIR) domains of the two receptors in close proximity to recruit myeloid differentiation 88 (MyD88) with the aid of TRIF-related adaptor molecule (TRAM) [10]. MyD88 further interacts with IL-1R-associated kinase (IRAK) to form a larger molecular complex that activates inhibitory κB kinase (IKK) via tumor necrosis factor receptor-associated factor 6 (TRAF6), and mitogen-activated protein kinase (MAPK) pathway effectors, including p38 MAPK and stress-activated protein kinase (SAPK/JNK) [11]. These signaling pathways culminate in the activation of NF-κB and other transcription factors, which induce both anti- and pro-inflammatory cytokines [12−17].

The pro-inflammatory activity of the IL-18/IL-18Rα/IL-18Rβ ternary complex is regulated by several additional secreted proteins. IL-37 [18,19], another member of the IL-18 cytokine subfamily, acts as an anti-inflammatory cytokine by forming a ternary complex with IL-18Rα and IL-1R8 (SIGIRR or TIR8), and thus sequestering IL-18Rα from the IL-18 signaling complex [20]. IL-18 binding protein (IL-18BP) [21] binds with very high affinity to IL-18 and has been shown to neutralize IL-18-mediated induction of IFN-γ in mice challenged with lipopolysaccharide [21]. However, IL-18BP can also bind IL-37 and could thus serve as a positive regulator of IL-18 signaling under some conditions [21]. Thus, proper immune and inflammatory responses to IL-18 depend not only on the cytokine itself but also on the interactions involving at least three cell-surface receptors (IL-18Rα, IL-18Rβ, and IL-1R8) and two secreted proteins (IL-37 and IL-18BP).

In spite of the importance of IL-18 signaling in many disease processes, to date, there have been only a few publications reporting inhibitory antibodies against IL-18 receptors. These include mouse monoclonal [22] and rabbit polyclonal [23] antibodies targeting the human IL-18Rα, and rat monoclonal antibodies targeting the mouse IL-18Rβ [24].

Here, we report the development of synthetic human antibodies that target human IL-18Rβ and block IL-18-mediated IFN-γ secretion by inhibiting NF-κB and MAPK dependent pathways. The crystal structure of a potent antagonist antibody in complex with IL-18Rβ revealed inhibition through an unexpected allosteric mechanism. The antibody bound to the backside of the receptor, away from the IL-18 and IL-18Rα binary complex binding site, and caused a large conformational change that prevented the formation of the ternary signaling complex. To our knowledge, this is the first report of an antibody antagonizing an interleukin receptor through an allosteric mechanism. Our findings offer a novel means for therapeutic intervention in the IL-18 pathway and may provide a new strategy for targeting interleukin receptors.

Results

Selection and characterization of antibodies binding to human IL-18Rβ

A phage-displayed library (Library F) of synthetic, human antigen-binding fragments (Fabs) was selected for binding to immobilized IL-18Rβ extracellular domain (ECD) [25]. Several hundred individual clones were assessed for antigen binding by phage ELISA, and positive clones were identified as those that bound to IL-18Rβ ECD but not to negative control proteins [26]. The DNA sequencing of positive clones revealed 19 unique Fabs that bound selectively to IL-18Rβ (Fig. S1).

The 19 Fab proteins were purified, and binding to IL-18Rβ ECD was assessed by ELISA over a range of Fab concentrations. Seventeen of the Fabs exhibited virtually no binding to negative control proteins (Fc or BSA) and saturable binding to human IL-18Rβ ECD, enabling determination of reliable EC_{50} values (Fig. S1A). Sequence comparisons revealed that most of the Fabs contained short CDR-H3 loops of identical length, suggesting that they all recognize antigen in a similar manner. However, two Fabs contained CDR-H3 loops of medium length with significant homology, suggesting similar binding mechanisms, and a single Fab contained a unique long CDR-H3 loop, suggesting a unique binding mechanism. Thus, based on comparison of sequences and EC_{50} values, we focused further characterization on one Fab with a short CDR-H3 (3132), one of the two Fabs with a medium-length CDR-H3 (3131) and the Fab with a unique long CDR-H3 (A3) (Fig. 1A and Fig. S1B).

For these three Fab proteins, in addition to determining EC_{50} values by direct binding ELISAs (Fig. 1B and Fig. S2A), we also determined IC_{50} values that quantified competition of solution-phase IL-18Rβ with immobilized IL-18Rβ for binding to solution-phase Fab (Fig. 1B and Fig. S2C). To corroborate this data, Fab binding kinetics were determined by biolayer interferometry (BLI), which showed the highest affinity for Fab 3131 ($K_D = 6.1$ nM), less tight but still high affinity for Fab 3132 ($K_D = 10$ nM) and modest affinity for Fab A3 ($K_D = 30$ nM), in general accord with ELISA data (Fig. 1B and Fig. S2E).

To characterize epitopes, we purified the three antibodies in the human IgG1 format. We performed blocking ELISAs to assess whether different antibodies could bind simultaneously by first incubating immobilized IL-18Rβ with saturating Fab protein and then detecting binding of IgG (Fig. 1C). As expected,
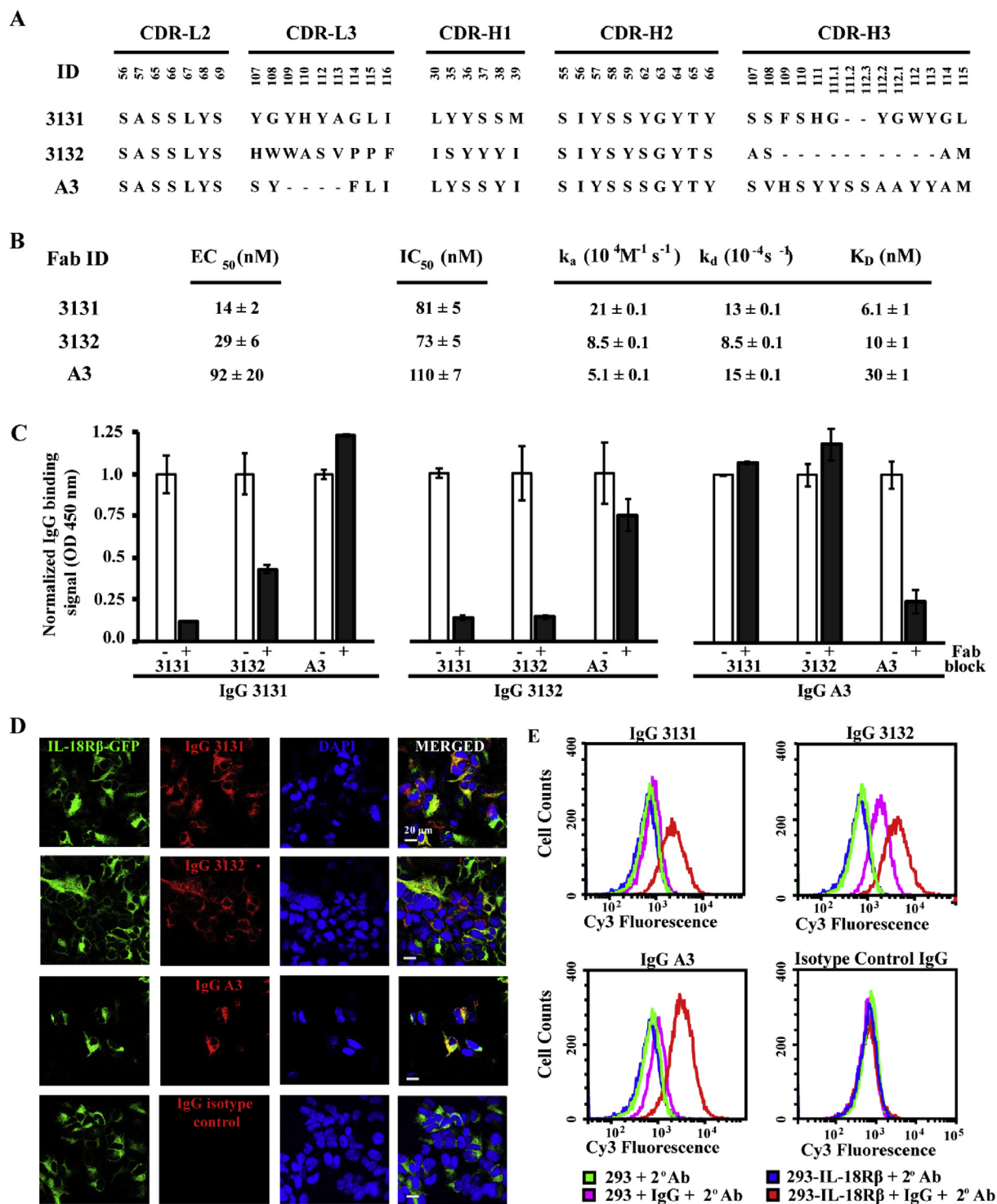
A

ID	CDR-L2	CDR-L3	CDR-H1	CDR-H2	CDR-H3
	56 57 65 66 67 68 69	107 108 109 110 112 113 114 115 116	30 35 36 37 38 39	55 56 57 58 59 62 63 64 65 66	107 108 109 110 111 111.1 111.2 112.3 112.2 112.1 112 113 114 115
3131	S A S S L Y S	Y G Y H Y A G L I	L Y Y S S M	S I Y S S Y G Y T Y	S S F S H G - - Y G W Y G L
3132	S A S S L Y S	H W W A S V P P F	I S Y Y Y I	S I Y S Y S G Y T S	A S - - - - - - - - - - A M
A3	S A S S L Y S	S Y - - - - F L I	L Y S S Y I	S I Y S S S G Y T Y	S V H S Y Y S S A A Y Y A M

B

Fab ID	EC_{50} (nM)	IC_{50} (nM)	k_a ($10^4 M^{-1} s^{-1}$)	k_d ($10^{-4} s^{-1}$)	K_D (nM)
3131	14 ± 2	81 ± 5	21 ± 0.1	13 ± 0.1	6.1 ± 1
3132	29 ± 6	73 ± 5	8.5 ± 0.1	8.5 ± 0.1	10 ± 1
A3	92 ± 20	110 ± 7	5.1 ± 0.1	15 ± 0.1	30 ± 1

Fig. 1. Anti-IL-18Rβ antibody sequences and binding characteristics. (**A**) The sequences of the CDRs are shown numbered according to IMGT standards [56], and dashes indicate gaps in the alignment. (**B**) Fab affinities for IL-18Rβ. EC_{50} and IC_{50} values were determined by ELISA, whereas kinetic constants (k_a and k_d) and the equilibrium dissociation constant (K_D) were determined by BLI. (**C**) To assess relative epitopes, binding of sub-saturating concentrations of IgG (1, 1 and 10 nM for 3131, 3132 or A3, respectively) to immobilized hIL-18Rβ was measured by ELISA in the absence (white bars) or presence (black bars) of a saturating concentration of Fab (0.25, 0.5 and 1 μM for 3131, 3132 or A3, respectively). Error bars represent the standard deviation (SD) of four replicate measurements. (**D**) IgG binding to cell surface receptors on HEK293-IL-18Rβ cells was assessed by immunofluorescence microscopy imaging of fluorescent signals from GFP expression (green) and IgG-binding (red) and the resultant images merged in the far-right column with DAPI-stained nuclei (blue) provided for contrast. (**E**) IgG binding to cell surface receptor binding was also characterized by flow cytometry using HEK293 or HEK293-IL-18Rβ cells versus isotype control IgG or secondary antibody alone.

each Fab protein blocked the binding of its own IgG. In addition, antibodies 3131 and 3132 blocked each other, whereas they neither blocked or could be blocked by antibody A3. These results suggest that antibodies 3131 and 3132 likely bind to overlapping epitopes, whereas antibody A3 binds to a distinct epitope that does not overlap with those of antibodies 3131 and 3132. EC_{50} and IC_{50} values of the three antibodies in the human IgG1 format were also determined (Fig. S2B and Fig. S2D).

We next assessed whether the IgGs could recognize full-length, cell-surface IL-18Rβ. For this purpose, we used HEK293 cells that were transiently transfected with a plasmid designed to express full-length IL-18Rβ with a C-terminal GFP fusion (HEK293-IL-18Rβ cells). Immunostaining followed by imaging with fluorescence microscopy showed extensive, but not completely coincident fluorescence for GFP and IgGs 3131, 3132, and A3, and no staining for a nonbinding isotype control IgG (Fig. 1D). The receptor-expressing cell regions that did not stain with antibody may reflect differences in antibody affinity, but immunofluorescence results agree closely with flow cytometry data, which also showed that IgGs 3131, 3132, and A3 labeled HEK293-IL-18Rβ cells (Fig. 1E). Moreover, IgGs 3131 and A3 did not label untransfected HEK293 cells, whereas IgG 3132 did. Finally, an isotype control IgG did not label either HEK293-IL-18Rβ cells or untransfected HEK293 cells (Fig. 1E). These results, taken together, showed that IgGs 3131 and A3 bind to distinct epitopes of IL-18Rβ with high affinity and specificity, whereas IgG 3132 showed some nonspecific binding to cell surfaces. Thus, we focused on antibodies 3131 and A3 and investigated the effects of the two IgGs on IL-18 cell signaling.

Effects of anti-IL-18Rβ antibodies on IL-18 signaling

To assess the effects of the anti-IL-18Rβ antibodies on cell signaling, we first tested the effect of Fabs 3131 and A3 on IL-18-induced gene transcription via NF-κB [27] in HEK293 cells transfected with a vector designed to express IL-18Rβ and a vector containing a luciferase gene under the control of NF-κB [9]. Both Fabs inhibited NF-κB transcriptional activity and luciferase signals induced by IL-18 (Fig. 2A). Next, we tested the effects of the IgGs on IL-18-induced secretion of IFN-γ, which was detected and quantified from cell supernatants by ELISA. Isolated PBMCs or KG-1 (human bone marrow acute myelogenous leukemia macrophage) cells, known to secrete IFN-γ in response to IL-18 [28,29], were pre-incubated with anti-IL-18Rβ IgG and then stimulated with IL-18 in combination with either IL-12 (10 ng/mL) for PBMCs or TNF-α (20 ng/mL) for KG-1 [30] (Fig. 2B). IgG 3131 inhibited IFN-γ

secretion in a dose-dependent manner in both KG-1 cells ($IC_{50} = 3 \pm 2$ nM) and PBMCs ($IC_{50} = 4 \pm 2$ nM), and inhibition was almost complete at high IgG concentrations, while IgG1 control had no effect on IL-18-induced IFN-γ secretion in both KG-1 cells and PBMCs. IgG A3 also inhibited IFN-γ secretion, but its effect was more variable among trials, and complete inhibition was not observed even at the highest concentrations tested, and thus, accurate IC_{50} values could not be determined. At the levels of cytokine used in our experiments, neither TNF-α nor IL-12 exerted effects on IFN-γ production in the absence of IL-18 (Fig. S3). Consistent with its strong antagonistic effects on IL-18 signaling, IgG 3131 inhibited binding of soluble IL-18/IL-18Rα to immobilized IL-18Rβ by ELISA, indicating that the antibody blocks formation of the ternary signaling complex (Fig. 2C).

Finally, we used western blotting to determine whether the anti-IL-18Rβ antibodies affected the phosphorylation levels of IKKα/IKKβ and p38 MAPK, which are known to be activated in response to IL-18 [31], and their downstream effector SAPK/JNK. As reported previously [31], brief stimulation of KG-1 cells with IL-18 caused increased phosphorylation of all three kinases, in comparison with basal phosphorylation in the absence of IL-18 (Fig. 2D). Pretreatment of the KG-1 cells with IgG 3131, prior to treatment with IL-18, reduced phosphorylation of all three kinases to basal levels, whereas pretreatment with IgG A3 did not (Fig. 2E). These results, taken together, show that IgG 3131 blocks binding of IL-18Rβ to the IL-18/IL-18Rα complex and is much more potent than IgG A3 as an antagonist of IL-18 signaling. The greater potency of IgG 3131 compared with IgG A3 may be due to higher affinity, differences in epitopes, or a combination of the two.

The structure of IL-18Rβ in complex with scFv 3131

The crystallization of IL-18Rβ in complex with the antibody was conducted to study the antagonistic mechanism of antibody 3131 against IL-18Rβ. The complex comprised of the hIL-18Rβ ECD and Fab 3131 failed to crystallize; however, crystals in the space group $P3_1$ were obtained from a complex of the receptor ECD and a single-chain variable fragment (scFv) version of the antibody, and these diffracted to 3.3 Å resolution (Table 1). Molecular replacement was used to determine the complex structure. The asymmetric unit (ASU) of the crystal contained three copies of the complex with chains A, B, and C (IL-18Rβ) bound to chains D, E, and F (scFv 3131), respectively (Fig. S4). Overall, the three complexes in the ASU had similar conformations. The average root-mean-square deviation (RMSD) of pairwise Cα within the three copies of IL-18Rβ was 1.5 Å while the average RMSD of pairwise Cα within
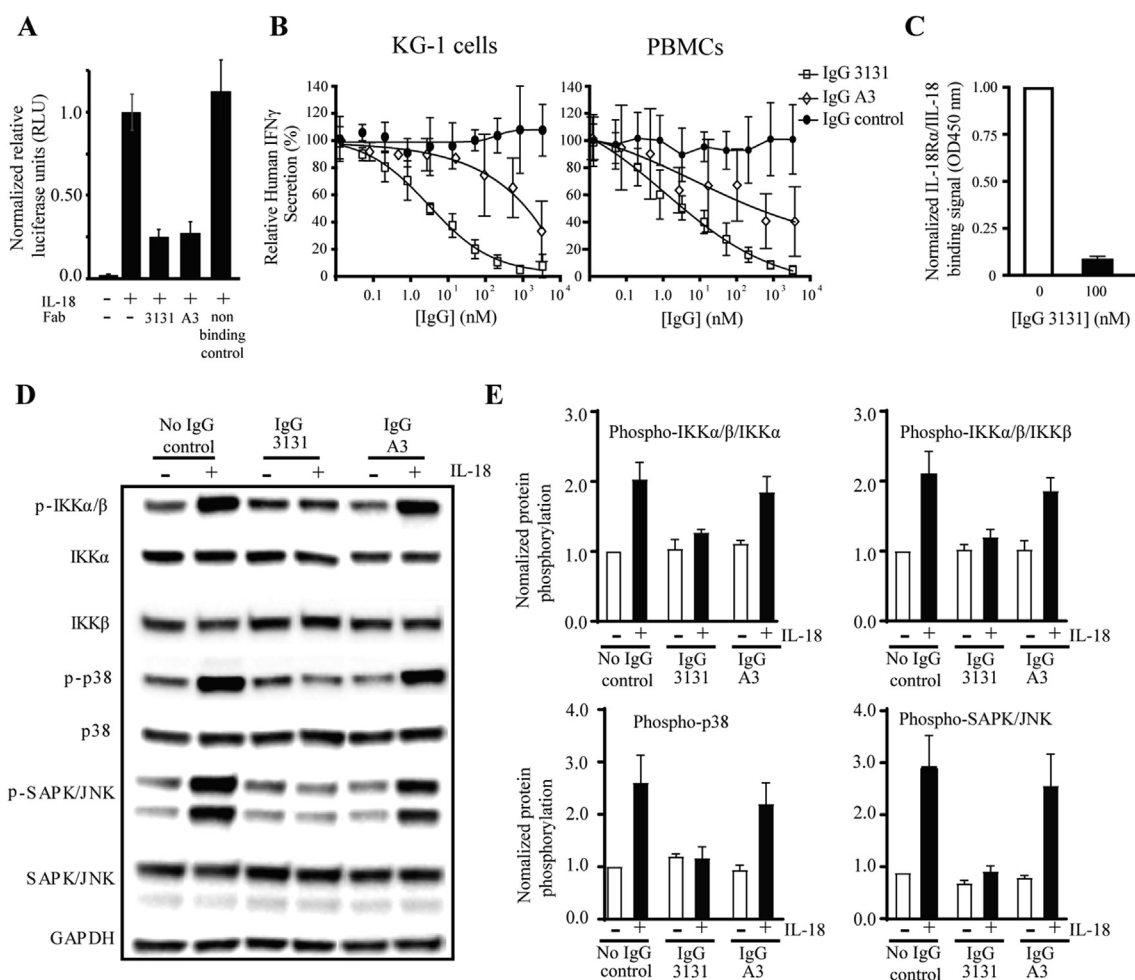
Fig. 2. Effects of anti-IL-18Rβ antibodies on IL-18 signaling. **(A)** Fab-mediated inhibition of IL-18-inducible luciferase signals under the control of an NF-κB response element was assessed by comparison to signals obtained in the absence of Fab or presence of nonbinding Fab control. Error bars represent the SD of triplicate measurements of luciferase signals normalized to cells treated with IL-18 alone. **(B)** IgG-mediated inhibition of IFN-γ secretion from either KG-1 cells (treated with 10 ng/mL IL-18 and 20 ng/mL TNFα) or PBMCs (treated with 50 ng/mL IL-18 and 10 ng/mL IL-12) was evaluated by sandwich ELISA. The mean and SD values of relative IFN-γ secretion were determined from 5 (KG-1) or six (PBMCs) independent experiments. **(C)** Inhibition of immobilized IL-18Rβ binding to a mixture of IL-18 (0.5 μg/mL) and IL-18Rα (2 μg/mL) (y-axis) by IgG 3131 (x-axis) was assessed by ELISA. **(D)** Antibody-mediated inhibition of IL-18-induced protein phosphorylation was assessed by western blotting of KG-1 cell lysates with anti-phospho-IKKα/β, -p38 MAPK, or -SAPK/JNK antibodies or antibodies to parent proteins. **(E)** Protein phosphorylation signals were determined by densitometry as the ratio of signals from phosphorylated protein to the corresponding total protein signal and normalized to the no IL-18 control. The mean and SD values are plotted as bar graphs with error bars from three independent experiments.

the three copies of scFv 3131 was 1.2 Å. The model was refined to a R_{work} and R_{free} of 25.1 and 27.8 respectively, and in the analysis that follows, we used the complex of chains A/D, unless otherwise noted. Some residues in chains A/D were not visible in the electron density map and were assumed to be disordered. These include residues 20−27, 52−94, 116−118, 128−138, 154−157 and 180−185 in IL-18Rβ, the linker between the heavy-chain variable domain (VH) and light-chain variable domain (VL), residues 122−123 in the VH domain, and residues 1−7, 27−29 and 109−110 in the VL domain.

Human IL-18Rβ ECD consists of three immuno-globulin-like (Ig) domains with the following boundaries: D1 (residues 20−150), D2 (residues 153−243), and D3 (residues 250−356) (Fig. 3A). The linker between D1 and D2 is short, and thus, these domains act as a D1-D2 module [9], whereas the linker between D2 and D3 is longer, which may allow for more conformational freedom between D1-D2 and D3. In the refined structure, D1 is the least ordered, as electron density is not well defined and the average B-factor is high (73 Å^2), in comparison to D2, which is more ordered with a lower average B-

Table 1. Data collection and refinement statistics.

Data collection	IL-18Rβ in complex with scFv 3131
Space group	P3$_1$
Unit cell dimensions	
a, b, c (Å)	163.16, 163.16, 64.15
α, β, γ ()	90, 90, 120
Wavelength (Å)	0.978
Resolution (Å)[a]	50.00−3.30 (3.42−3.30)
Observed reflections	96462
Unique reflections	28309
Completeness (%)	98.6 (95.3)
R$_{merge}$ (%)	11.3 (65.2)
<I/σ(I)>	11.5 (1.8)
Redundancy	3.4
Refinement statistics	
Resolution range (Å)	39.19−3.30
No. of molecules/ASU	6
R$_{work}$/R$_{free}$ (%)[b]	25.1/27.8
No. of atoms	9768
Mean B value	50.1
RMSDs	
Bond length (Å)/bond angle ()	0.011/1.376
Ramachandran plot (%)[c]	80.4/19.6/0

Crystallographic data and refinement statistics.

[a] Values in the highest resolution shell are shown in parentheses.

[b] R$_{work}$ = Σ||Fobs| − |Fcalc||/Σ|Fobs|. R$_{free}$ is calculated identically, with 5% of randomly chosen reflections omitted from the refinement.

[c] Fractions of residues in most favored/allowed/disallowed regions of the Ramachandran plot were calculated using PROCHECK.

factor (61 Å^2) and to D3, which is the most ordered with the lowest average B-factor (28 Å^2). Asn345 in D3 is directly linked to N-acetyl-D-glucosamine (NAG), in agreement with previous reports [9].

In the complex, D1 does not interact with scFv 3131. D2 and D3 interact with the light-chain variable domain (VL) and the heavy-chain variable domain (VH), respectively, whereas the D2-D3 linker interacts with both VL and VH (Fig. 3A). The NAG linked to Asn345 does not interact with scFv 3131. Notably, the total buried surface areas vary amongst the three complexes in the ASU, as 1997 Å^2, 1700 Å^2, and 2140 Å^2 are buried in chains A/D, B/E, and C/F, respectively. This variance amongst the three superposed complexes was due to the rotation (3.9°−13.1°) of D1-D2 with respect to D3 (Fig. S5), suggesting that the D2-D3 linker is flexible in solution.

Interface between IL-18Rβ and scFv 3131

The binding of scFv 3131 to IL-18Rβ results in an extensive interface, with 1012 and 985 Å^2 of surface area buried on the antibody paratope and the antigen epitope, respectively (Fig. 3B). The IL-18Rβ epitope is centered on the D2-D3 linker, flanked on either side by D3 and D2, which contribute 695 and 277 Å^2 of buried surface area,

respectively. The antibody paratope is dominated by CDR-H3, which contributes 533 Å^2 of buried surface area, and is supported on one side by CDR-H1 (247 Å^2) and on the other side by CDR-L2 (143 Å^2).

Notably, scFv 3131 recognizes IL-18Rβ by using not only residues that were diversified in the library CDR-H1 and CDR-H3 design, but also, residues that were fixed in CDR-H1, CDR-H3, CDR-L2 and in the framework regions (FRs). For instance, extensive polar interactions are made by both diversified residues (Ser108[H], His111[H], and Tyr113[H]) and fixed residues (Arg106[H] and Asp116[H]) in the CDR-H3 loop (Fig. 3C). The side chain of Arg106[H] hydrogen bonds with the main-chain carbonyl group of Arg281, while the side chain of Asp116[H] forms a salt bridge with the side chain of Arg281 and the main-chain carbonyl of Tyr113[H] hydrogen bonds with the main chain of Arg281. His111[H] establishes a hydrogen-bonding network with the main-chain carbonyl of Gly278 and the side chains of Ser310 and Glu315 in D3. In CDR-H1, the main-chain carbonyl and amine groups of fixed residues Gly27[H] and Asn29[H], respectively, form hydrogen bonds with the side chain of Asn284, and the side chain of the diversified residue Tyr36[H] forms hydrophobic interactions with Phe283, Pro285, and Ile317 (Fig. 3D). Although CDR-L2 was fixed in the library, the loop and surrounding framework also significantly
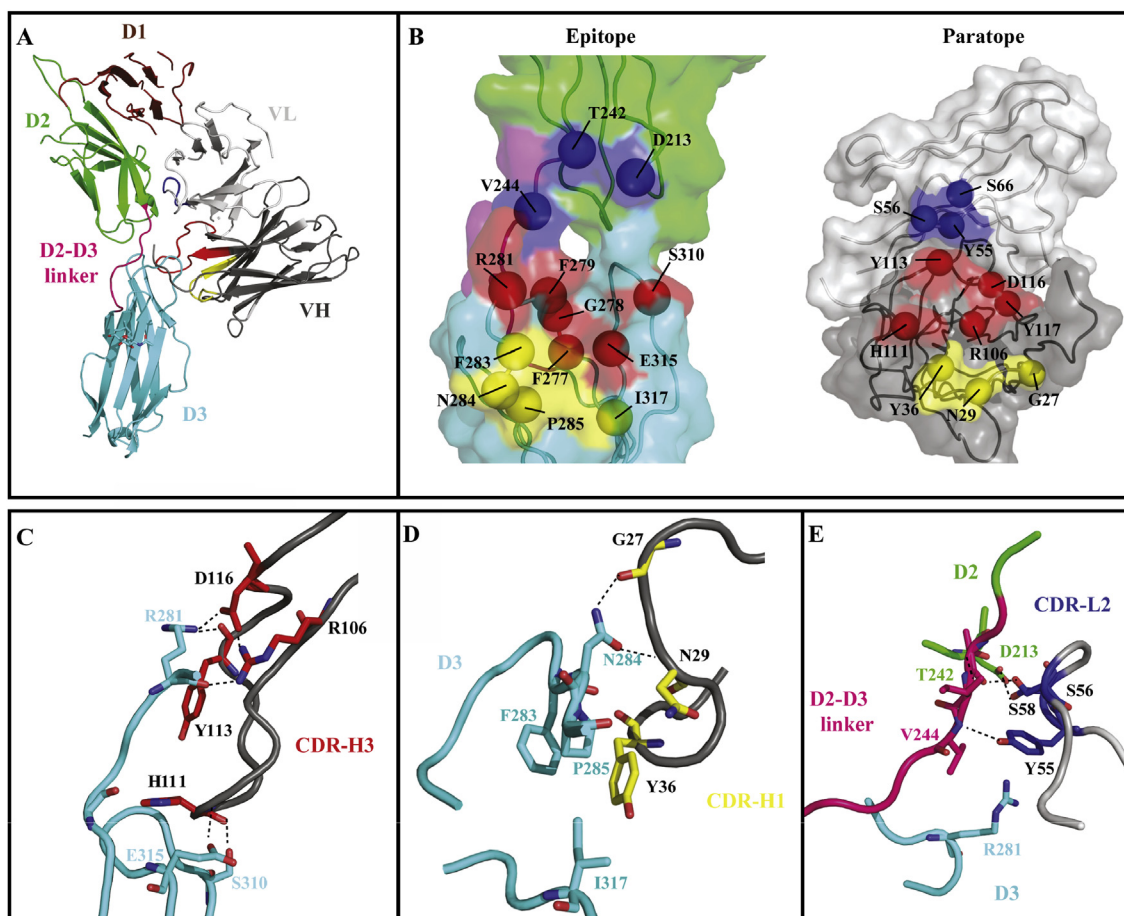
Fig. 3. The crystal structure of the IL-18Rβ-scFv 3131 complex. (A) The overall structure of the IL-18Rβ-scFv 3131 complex. IL-18Rβ domains are colored as follows: D1 (brown), D2 (green) D2-D3 linker (magenta), D3 (cyan). The scFv variable domain heavy and light chains are colored light and dark grey, respectively, and the CDRs are colored as follows: CDR-L2 (blue), CDR-H1 (yellow), and CDR-H3 (red). The NAG, linked to Asn345 in the D3 domain, is shown as sticks. **(B)** The structural epitope and paratope. IL-18Rβ (left) and scFv 3131 (right) are shown in open book view as molecular surfaces. Residues that make contact at the interface are represented by spheres. scFv 3131 paratope residues are colored the same as in (A) if they contact IL-18Rβ. IL-18Rβ epitope residues are similarly colored blue, yellow, or red if they contact CDR-L2, CDR-H1, or CDR-H3, respectively. **(C-E)** Molecular details of interactions between IL-18Rβ and **(C)** CDR-H3, **(D)** CDR-H1, and **(E)** CDR-L2 Dashed lines represent hydrogen bonds or salt bridges.

contribute to binding (Fig. 3E). The side chains of Ser56^L and S66^L form hydrogen bonds with the side chain of Asp213 and the main-chain carbonyl group of Thr242, respectively. Lastly, the side chain of Tyr55^L forms a cation-pi interaction with the side chain of Arg281 and hydrophobic interactions and a hydrogen bond with the side and main chain of Val244, respectively.

Finally, numerous Van der Waals contacts augment the antibody-antigen interaction. On the antibody side, these are contributed by diversified (Tyr36^H from CDR-H1 and Tyr113^H from CDR-H3) and fixed positions (Phe28^H from CDR-H1, Tyr117^H from CDR-H3 and Tyr55^L from FR2). On the antigen side, these are contributed by D3 (Phe277, Phe279, Val282, Phe283, Pro285, Leu312, Ile317), and the D2-D3 linker (Val244) (Fig. 3C, D and E).

Comparison of the IL-18Rβ/scFv 3131 complex with the IL-18/IL-18Rα/IL-18Rβ ternary complex

To understand how antibody 3131 blocked binding of IL-18Rβ to the IL-18/IL-18Rα complex and inhibited IL-18 signaling (Fig. 2), we compared the epitopes on IL-18Rβ for binding to scFv 3131, IL-18Rα and IL-18 (Fig. 4A). While scFv 3131 and IL-18Rα make extensive contacts with IL-18Rβ, the two epitopes do not overlap and are on opposite sides of IL-18Rβ (Fig. 4A), and moreover, the epitope for IL-18 shows no overlap with the scFv 3131 epitope. Thus, there is no overlap between the epitope on IL-18Rβ for scFv 3131 and those for IL-18Rα and IL-18, suggesting strongly that the antagonistic activity of the antibody is not due to direct steric blockade of the ternary complex.
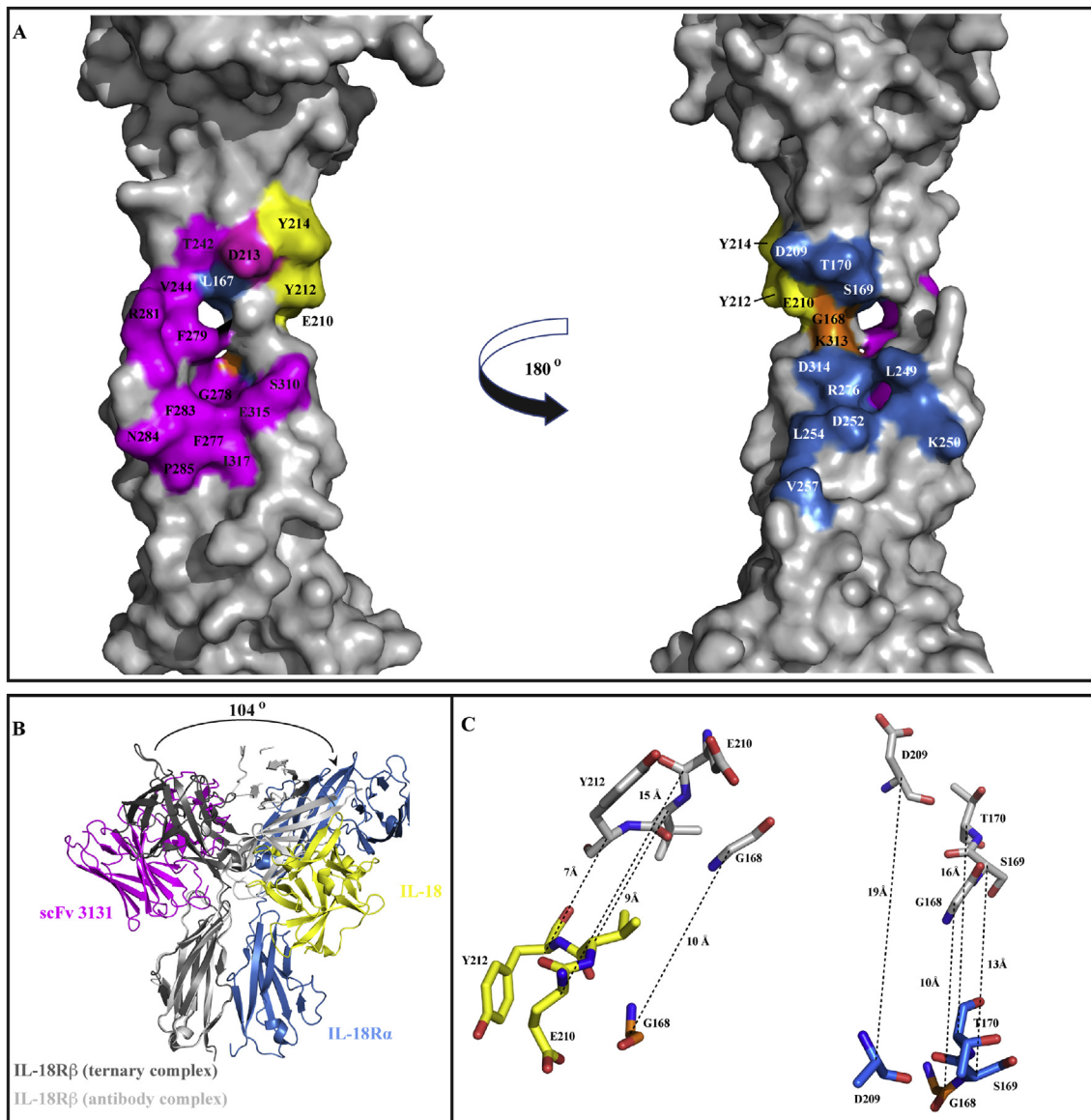
Fig. 4. Comparison of the IL-18Rβ/scFv 3131 and IL-18/IL-18Rα/IL-18Rβ ternary complex structures. **(A)** Structural epitopes for binding to scFv 3131 (magenta), IL-18Rα (blue) or IL-18 (yellow) mapped on the surface IL-18β from the IL-18Rβ/scFv 3131 complex structure. A residue was considered to be part of a structural epitope if any atoms were within 3.5 Å of any atoms in the binding partner. Gly 168 and Lys313 (orange) are shared by the epitopes for IL-18 and IL-18Rα. **(B)** Superposition of the IL-18Rβ/scFv 3131 complex on to the IL-18/IL-18Rα/IL-18Rβ ternary complex (PDB code: 3WO4), performed using the D3 domains of the two IL-18Rβ molecules as reference. In the IL-18Rβ/scFv 3131 complex, IL-18Rβ is colored light grey, and scFv 3131 is colored magenta. In the IL-18/IL-18Rα/IL-18Rβ complex, IL-18 is colored yellow, IL-18Rα is colored blue, and IL-18Rβ is colored dark grey. The D1-D2 module of IL-18Rβ undergoes a 104° rotation relative to the D3 domain in the two structures. **(C)** Relative positions of IL-18Rβ residues in the epitopes for binding to IL-18 or IL-18Rα within the superposition in panel (B). Residues in the IL-18 or IL-18Rα epitope mapped on the IL-18Rβ from IL-18Rβ/scFv 3131 complex are colored yellow or blue, respectively, whereas those mapped on the IL-18Rβ from IL-18/IL-18Rα/IL-18Rβ ternary complex are colored grey. Distances between corresponding Cα atoms are represented by dashed lines.

Next, we explored whether the antagonist activity of antibody 3131 was mediated by an allosteric mechanism. We superposed our structure with a previously reported structure of the IL-18/IL-18Rα/IL-18Rβ ternary complex (Fig. 4B) [9]. The superposition of the D3 domains in the two structures revealed a large rotation of 104° for the relative orientation of the D1-D2 module along with a tri-

peptide linker (Val244-Gly245-Asp246). To our knowledge, this is the first report that the D2-D3 linker of IL-18Rβ may be flexible and could thus facilitate significant movement between the D2 and D3 domains. Importantly, this large relative rotation dramatically alters the positions of key residues in D2, which contribute to the epitopes for IL-18 and IL-18Rα, such that binding of scFv 3131 is clearly incompatible with interactions in the ternary complex. For example, between the two superposed structures, the positions of the Cα atoms of Glu210 and Tyr212, which contact IL-18, differ by 15 Å, and those of Ser169, Thr170, and Asp209, which contact IL-18Rα, differ by 13−19 Å (Fig. 4C). These observations, taken together, show that the antagonistic activity of antibody 3131 is caused by an allosteric mechanism, whereby rotation of the D1-D2 module relative to the D3 domain results in a conformation that is incompatible with the formation of the ternary IL-18/IL-18Rα/IL-18Rβ signaling complex.

Discussion

Previous reports have described antibodies against human [22] and mouse IL-18Rα [23] or mouse IL-18Rβ [24], and allosteric antibodies against a cytokine receptor (prolactin receptor) [32]. However, to our knowledge, antibody 3131 is the first to target human IL-18Rβ and is the first to inhibit an interleukin receptor in an allosteric manner. Inhibition of inflammatory signals is a widespread aim in drug development, given their role in various inflammatory diseases, including intestinal bowel disease, diabetes, pulmonary disorders, and others. Allosteric antagonists offer appeal as therapeutic modulators by targeting regions that are typically more diverse than conserved ligand binding sites, thus, potentially providing better selectivity. Further, blockade of IL-18Rα increased inflammatory cytokines as a result of the loss of IL-37-mediated anti-inflammatory signaling, which also employs IL-18Rα as a co-receptor [33]. Consequently, the dual role of IL-18Rα in both IL-18 and IL-37 signaling complicates the use of IL-18Rα blockade as an anti-inflammatory strategy, and targeting IL-18Rβ may prove to be more selective and efficacious.

To our surprise, elucidation of the structure of scFv 3131 in complex with IL-18Rβ revealed that the antibody stabilizes a large rotational change between the D1-D2 module relative to D3. Although interdomain flexibility between the D1-D2 module and D3 is generally recognized as a common feature of the ligand-binding components of the IL-1 family of receptors (IL-1R, IL-18R, ST2, 1L-36R), it is less clear for the accessory proteins of the family for which, to our knowledge, no uncomplexed structures or evidence of dynamic conformational sampling

exist. Within the IL-1 family, IL-1Rβ, the accessory protein for several ligand-binding receptors (IL-1R, IL-33R, IL-36R), bears a similar three-domain structure and function as IL-18Rβ, in that it makes few direct contacts with cytokine relative to the ligand-binding component, but rather acts as an accessory signaling component. However, a previous study of IL-1Rβ has suggested, despite the presence of an analogous linker and similar paucity of apparent interdomain interactions, that structural rigidity is maintained between the D1-D2 module and D3 [34]. Since IL-1Rβ is a partner for three different receptors in the IL-1 family, this lack of flexibility would pose limitations to the potential for allosteric modulation within this family.

In light of this and in the absence of data on the conformational dynamics of IL-18Rβ, the degree of flexibility revealed by our structure highlights differences between the two accessory proteins that can be exploited for the development of allosteric antagonists. In this manner, IL-18Rβ appears to share the flexibility more often observed in the ligand-binding receptors of the IL-1 family.

Given the recognized flexibility of the ligand-binding receptors, other members of the IL-1 family may be susceptible to allosteric antagonism analogous to the effects of antibody 3131 on IL-18Rβ. The IL-1 receptor family contains 10 members, (IL-1R1-10) [1] and all family members—with the exception of IL-1R8 (SIGIRR), which contains a single Ig-like domain—contain three Ig-like domains in their ECD, and these all contain fairly long linkers, comprised of 8−11 residues, between the D1-D2 module and D3 (Figs. S6 and S7). In further support of a susceptibility to allosteric antagonism, SAXS studies of the IL-1 family member ST2 have suggested that the ligand-binding subunit of the IL-33 receptor also possesses a range of conformational flexibility in the absence of ligand [33], and linker flexibility between the D2 and D3 domains has also been observed in other IL-1R complexes [35,36]. Inspection of the six receptors for which structures have been solved (including IL-1R1 [37], IL-1R2 [38], IL-1R4 [34], IL-1R5 (IL-18Rα) [9], IL-1R7 (IL-18Rβ) and IL-1R9 [39]) highlights the connection of the compact D1-D2 module to D3 through a linker (Fig. S7), suggesting that these receptors may also have multiple conformations due to inherent flexibility.

Moreover, the crystal structures of uncomplexed receptors within the IL-1 family have not been reported, possibly due to the dynamic conformations of these receptors that may make them resistant to crystallographic study. In agreement, our structure of IL-18Rβ in complex with scFv 3131, compared with the existing IL-18Rβ structure, showed that the extended linker is flexible and allows the D1-D2 module and the D3 domain to adapt different relative orientations. These findings support the notion that linker flexibility between the D2 and D3 domains may

be an inherent feature of the IL-1 receptor family, and thus, we speculate that antibodies that utilize an allosteric mode of inhibition similar to that observed for scFv 3131 could target other receptors in this family.

We have assessed the binding of IgG 3131 to rhesus IL-18Rβ ECD by surface plasmon resonance, as *in vivo* testing in this model system would be critical for advancing potential therapeutic applications. Although the human and rhesus IL-18Rβ ECDs share 92% sequence identity, the side chain of Asp213 in the human receptor is involved in a hydrogen-bonding interaction with scFv 3131, and this residue is substituted by an Ile residue in the rhesus receptor. Thus, we predicted that this difference would disrupt the hydrogen-bonding interactions, and consequently, may reduce affinity for rhesus IL-18Rβ. In agreement, we observed an approximately 10-fold lower affinity for the rhesus receptor relative to the human receptor (data not shown). However, the sequence at position 213 is the only difference between human and rhesus IL-18Rβ epitopes for scFv 3131, and thus, it should be possible to engineer variants of antibody 3131 with enhanced affinity for the rhesus receptor, and ideally, an equal affinity for both species. In this regard, the structure of scFv 3131 in complex with human IL-18Rβ provides an ideal template to aid the design of phage-displayed libraries of antibody 3131 variants that could be screened for species cross-reactive antagonists of IL-18Rβ activity for therapeutic evaluation.

Materials and Methods

Selection of anti-IL-18Rβ antibodies

Library F, a phage-displayed library of synthetic antigen-binding fragments (Fabs) [25], was used in selections for binding to the Fc-tagged extracellular domain (ECD) of human IL-18Rβ (IL-18Rβ-Fc) (R&D Systems) immobilized in 96-well NUNC Maxisorp immunoplates (Thermo Fisher Scientific), as described [40]. After four rounds of selections, phage from single colonies were tested for specific binding by phage enzyme-linked immunosorbent assay (ELISA), and clones that bound to IL-18Rβ-Fc but not to Fc were subjected to DNA sequencing to decode the sequences of the Fab complementarity-determining regions (CDRs), as described [26].

Antibody purification and ELISAs

Fab proteins were expressed and purified from *Escherichia coli* (*E. coli*) BL21, as described [41]. Variable heavy and light chain genes were sub-cloned into pFuse human IgG1 and κ vectors (Invivogen), respectively, and the resulting expression vectors were used to express and purify IgG1 proteins from HEK-293F suspension cells as described [41,42]. EC_{50} and IC_{50} values for Fabs binding to immobilized IL-18Rβ-Fc were determined by direct binding or competitive ELISAs, respectively, as described [43]. Simultaneous binding of antibodies to immobilized IL-18Rβ-His (Sino Biological Inc.) was evaluated to map relative epitopes using methods similar to those described [43], by blocking IL-18Rβ-His with saturating Fab protein and measuring subsequent binding of IgG protein with anti-Fc-HRP (Jackson Immunoresearch). Similarly, simultaneous binding of IgG and IL-18/IL-18Rα-Fc-His (R&D Systems) to immobilized IL-18Rβ-Fc was evaluated by blocking IL-18Rβ-Fc with saturating IgG and detecting binding of IL-18/IL-18Rα-Fc-His with anti-His-HRP antibody (Abcam). ELISA binding curves were fit in GraphPad Prism (Version 5.0) using the log (agonist) versus response-variable slope model or the log (inhibitor) versus response-variable slope model from which EC_{50} and IC_{50} estimates were obtained, respectively.

Biolayer interferometry

The binding kinetics of antibody interaction with IL-18Rβ-Fc were determined by biolayer interferometry (BLI) at 25 °C using a ForteBio Octet HTX system (Pall Corp.). Receptor (40 μg/mL) was immobilized on an AHQ biosensor (Pall Corp.) followed by 600 s association and 600 s dissociation of serial dilutions of Fab (6.25−400 nM) in PBT buffer (PBS, 1% BSA, 0.05% Tween 20). For all steps, samples were shaken at 1000 rpm. The binding curves were globally fit to a 1:1 Langmuir-binding model using nonlinear regression analysis with the Octet Data Analysis Software version 9.0 (Pall Corp.), and k_a and k_d values were determined from the association and dissociation phases, respectively. The equilibrium dissociation constant (K_D) was determined as the k_d/k_a ratio. Errors associated with the constants were determined as the standard deviation (SD) of the locally fit curves.

Cell culture

HEK293F cells (Thermo) were cultured in FreeStyle™ 293 Expression Medium (Gibco). HEK293 cells (ATCC) were plated in Dulbecco's Modified Eagle Medium (Gibco) supplemented with 10% fetal bovine serum (FBS) (Gibco). KG-1 cells (CCL-246, ATCC) were grown in Iscove's Modified Dulbecco's Medium (Gibco) containing 10% FBS. Human peripheral blood mononuclear cells from six healthy donors (PBMCs) were individually suspended in RPMI 1640 Medium (Gibco) plus 10% FBS. Cells were incubated at 37°C in a humidified atmosphere of 5% CO_2.

Immunofluorescence microscopy

HEK293 cells (1×10^5 suspended in 1 mL media) were plated on poly-D-lysine (Sigma) coated 14-mm glass coverslips (Thermo Scientific) in 24-well flat-bottom plates and allowed to adhere for 48 h. Cells were transfected with a plasmid expressing GFP-tagged, full-length IL-18Rβ, and allowed to grow 24 h before fixation. Cells were fixed in 4% paraformaldehyde (Solarbio), incubated 30 min in

blocking buffer (Thermo Scientific), incubated overnight at 4°C with 400 nM IgG, washed three times with PBS, and incubated with Cy3-conjugated goat anti-human IgG secondary antibody (1:500 dilution; 109-166-097, Jackson Immunoresearch). Cells on coverslips were mounted on glass slides (Thermo Scientific), treated with Prolong Gold with DAPI (Vector Laboratories), and imaged on an inverted microscope equipped with a confocal system (Zeiss LSM710), as described [43].

Flow cytometry

HEK293 cells transiently expressing IL-18Rβ−GFP were collected and resuspended in ice-cold wash buffer (PBS, 0.1% BSA). Resuspended cells (1×10^6 in 100 μL) were incubated for 1 h on ice with anti-IL-18Rβ IgG and incubated for 0.5 h with Cy3-conjugated goat anti-human IgG secondary antibody (1:500 dilution). After staining, 10^5 cells were analyzed by flow cytometry (CytoFLEX S, Beckman Coulter) after exclusion of debris, aggregates, and non-GFP expressing cells, and histograms of anti-IL-18Rβ antibodies were compared to a nonbinding isotype control IgG1 (HG1K, Sino Biological Inc.).

Luciferase reporter assay

Inhibition of IL-18-induced NF-κB signals by anti-IL-18Rβ antibodies was evaluated by luciferase assay, as described [9]. HEK293 cells (2×10^5 cells in 100 μL media) were plated in individual TM 96TC wells (PerkinElmer) and allowed to grow 48 h. Cells were transfected, using Lipofectamine 2000 or 3000 reagent (Invitrogen) according to manufacturer's instructions, with 100 ng of either the empty pcDNA3.1(+) vector (Invitrogen) or the same vector in to which the full-length IL-18Rβ gene had been cloned, along with both the pGL4.32 [luc2P/NF-κB-RE/Hygro] vector (Promega), which contains five copies of an NF-κB response element (NF-κB-RE) that drives transcription of the luciferase reporter gene *luc2p* (*Photinus pyralis*), and a control vector with no promotor (pGL4.7hRluc) (Promega), which encodes *hRluc* gene (*Renilla reniformis*). Transfected cells were incubated for 1 h with serial dilutions of IgG prior to stimulation for 6 h with IL-18 (10 ng/mL) (Sino Biological Inc.). The luciferase reporter gene activities were analyzed using the dual-luciferase reporter assay system (Promega) on an Enspire luminometer (Perkin Elmer).

Cytokine secretion assay

KG-1 cells (CCL-246, ATCC) (3×10^5 in 140 μL media) or human peripheral blood mononuclear cells (PBMCs; Milestone Biotechnologies) from six healthy donors (1×10^5 in 70 μL media) were plated in 96-well plates (Corning Inc.), as described [28]. Serial dilutions of IgG were applied to wells prior to stimulation for 1 h with 10 ng/mL human IL-18 plus 20 ng/mL human TNF-α (R&D Systems) (KG-1 cells) or 50 ng/mL IL-18 plus 10 ng/mL IL-12 (R&D Systems) (PBMCs). After 16−20 h (KG-1) or 72 h (PBMCs), cells were pelleted by centrifugation at 400*g*, and IFN-γ was measured from the supernatant using an ELISA kit (R&D Systems) according to manufacturer's instructions. The percentage of relative IFN-γ secretion was obtained by normalizing to a positive control (cytokines alone) after subtracting the background. The mean and the SD were calculated from five (KG-1) or six (PBMCs) independent experiments. IC_{50} values were estimated from the dose-response curves by curve fitting in GraphPad Prism (Version 5.0) using the [inhibitor] versus response (four-parameter variable slope) model. All cytokines were sourced from R&D Systems.

IL-18-induced phosphorylation assay

KG-1 cells (3×10^6 in 500 μL media) were plated in 48-well plates, serum starved for 4 h, incubated with 6.4 μM IgG for 1 h at 37°C, and stimulated with IL-18 (50 ng/mL) for 15 min. Cells were harvested by centrifugation at 400*g* for 5 min and the clear lysate was electrophoresed and transferred to PVDF solid supports for blotting, as described [31,43]. Blots were incubated overnight at 4°C with rabbit anti-human phospho-SAPK/JNK (4668; Cell Signaling), rabbit anti-human phospho-IKKα/β (2078, Cell Signaling), or rabbit anti-human phospho-38 MAPK (4631; Cell Signaling). The blots were incubated with secondary antibody, anti-rabbit IgG-HRP (7074; Cell Signaling), for 2 h at 4°C. Signals were visualized using enhanced chemiluminescence (Thermo Scientific), and scanned using the Bio-Rad Chemi-Doc imaging system (BioRad). The blots were stripped for 30 min at room temperature with stripping buffer (Beyotime), blocked for 2 h with milk, and re-probed with rabbit anti-human SAPK/JNK (9252; Cell Signaling), rabbit anti-human IKKα (2682; Cell Signaling), rabbit anti-human IKKβ (8943; Cell Signaling) or rabbit anti-human p38 MAPK (8690; Cell Signaling). Densitometry was used to compare western blot signals by measuring the grey density of individual bands. Grey densities of phospho-protein bands were normalized to total protein band (*e.g.* dividing phospho-p38/p38) for each lane and expressed relative to the normalized control, as described [44]. Three independent experiments were conducted to calculate the normalized protein phosphorylation from which mean and SD values were determined. Densitometry data for antibody and control treatments were statistically compared by One-way Analysis of Variance (ANOVA) with Bonferroni's Multiple Comparison as post hoc analysis using GraphPad Prism.

Protein purification for crystallization

A cDNA sequence encoding residues 20−356 of IL-18Rβ ECD was cloned into a modified pFastBac Dual vector (Life Technologies, Inc.) to generate a secreted N-terminal His fusion protein with a 3C protease cleavage site between 6xHis tag and hIL-18Rβ sequence, as described [45], but using *E. coli* DH10EMBacY for Tn7-mediated transposition into the bacmid [46]. High Five cells were used to express and purify the secreted IL-18Rβ ECD, as described [45]. Purified IL-18Rβ ECD was concentrated to 10 mg/mL in 20 mM HEPES, 100 mM NaCl, pH 7.5 buffer and stored in aliquots at −80 °C.

A DNA fragment encoding the scFv 3131 gene was converted from Fab-3131 by connecting the gene fragments of the variable domain of heavy and light chains (VH and VL) with a 17-residue Gly-Ser linker resulting in an scFv with VH-linker-VL architecture. It was cloned into a pETDuet-1 protein expression vector modified with the 23-residue StiI signal peptide (Sequence: MKKNIAFLLASMFVFSIATNAYA) [25] to generate a 6xHis fusion protein with a 3C protease cleavage site. The scFv 3131 protein was induced to express with 0.2 mM IPTG at 16°C with shaking at 200 rpm for around 12 h when the OD_{600} of *E. coli* BL21 (DE3) was ~0.6. The cells were pelleted by centrifugation, and the pelleted cells were resuspended and sonicated. The supernatant after centrifugation was purified using a similar strategy as that of IL-18Rβ ECD except for a polishing step on a Mono Q anion exchange column (GE Healthcare). The purified protein was concentrated to 10 mg/mL in 20 mM HEPES, 100 mM NaCl, pH 7.5 buffer, and stored in aliquots at −80 °C.

Purified IL-18Rβ and scFv 3131 proteins were mixed at 1:2 M ratio, incubated on ice for 1 h, and purified on an S200 26/600 column (GE Healthcare). The eluted complex was concentrated to 10 mg/mL in 20 mM HEPES, 100 mM NaCl, pH 7.5 buffer, and stored in aliquots at −80°C.

Protein crystallization, data collection, and structure determination

Crystals were grown using the sitting-drop vapor diffusion method with 60 μL reservoir solution in wells of a 96-well plate. 100 nL of protein sample was mixed with 100 nL of 0.2 M ammonium iodide and 20% (w/v) polyethylene glycol (PEG) 3350 at 15°C. Crystals were grown to full size in approximately 5 days and transferred from mother liquor to 0.2 M ammonium chloride, 25% (w/v) PEG 3350, 20% PEG 400 in serial steps before being flash-frozen into liquid nitrogen.

X-ray diffraction data from one single crystal were collected at beamline BL19U (Shanghai Synchrotron Radiation Facility, China), and were scaled and merged with HKL-3000 [47]. Molecular replacement was conducted using a Phaser in Phenix [48]. The scFv 3131 search model without CDRs was built based on a Fab with the same framework [25] (PDB code: 3PNW) in Swiss-Modeling [49]. Three copies of scFv 3131 were identified with a reliable Z score while using the whole human IL-18Rβ ECD as a search model (PDB code: 3WO4) failed to generate a reliable Z score. In contrast, by using human IL-18Rβ D1-D2 domains and D3 domain as distinct search models identified three copies of each with reliable Z scores. Iterative model building in Coot [50] and refinement in Phenix Rosetta Refine [48] and Refmac in CCP4 [51] was conducted to generate the final models of IL-18Rβ in complex with scFv 3131. The stereochemical geometry of the models was checked using PROCHECK [52]. Structural figures were prepared using Pymol (www.pymol.org). Root-mean-square deviations (RMSD) and buried solvent accessible surface areas were calculated in the Dali server [53] and Protein Interactions Calculator Server [54], respectively. Domain rotation was analyzed in Dyndom [55].

Additional information

Accession code

The coordinates and structure-factor amplitudes of IL-18Rβ in complex with scFv 3131 have been deposited to PDB with accession code 6KN9.

Author contributions

S.S. and D.W. conceived, designed, and supervised the study. S.L, S.M., P.L. B.B, J.S, H.H., and J.P. performed panning, biophysical, and biochemical characterization of antibodies. C.L. performed the crystallization of IL-18Rβ in complex with scFv 3131. W.Q. collected the crystallographic X-ray diffraction data and processed the data. D.W. solved, refined, and analyzed the structure of IL-18Rβ in complex with scFv 3131. S.L., S.M., S.S., and D.W. wrote and revised the manuscript.

Conflict of interest statement

S·S., D.W., S.L., S.M., H.H., and J.P. applied a patent (PCT/CN2019/091936) for these antagonistic antibodies.

Appendix A. Supplementary data

Supplementary data to this article can be found online at https://doi.org/10.1016/j.jmb.2020.01.012.

References

[1] C.A. Dinarello, Overview of the IL-1 family in innate inflammation and acquired immunity, Immunol. Rev. 281 (2018) 8−27.

[2] G. Kaplanski, Interleukin-18: Biological properties and role in disease pathogenesis, Immunol. Rev. 281 (2018) 138−153.

[3] D. Novick, S. Kim, G. Kaplanski, C.A. Dinarello, Interleukin-18, more than a Th1 cytokine, Semin. Immunol. 25 (2013) 439−448.

[4] S. Akira, The role of IL-18 in innate immunity, Curr. Opin. Immunol. 12 (2000) 59−63.

[5] I.B. McInnes, J.A. Gracie, B.P. Leung, X.Q. Wei, F.Y. Liew, Interleukin 18: a pleiotropic participant in chronic inflammation, Immunol. Today 21 (2000) 312−315.

[6] K. Nakanishi, T. Yoshimoto, H. Tsutsui, H. Okamura, Interleukin-18 is a unique cytokine that stimulates both Th1 and Th2 responses depending on its cytokine milieu, Cytokine Growth Factor Rev. 12 (2001) 53−72.

[7] F. Vidal-Vanaclocha, L. Mendoza, N. Telleria, C. Salado, M. Valcarcel, N. Gallot, et al., Clinical and experimental approaches to the pathophysiology of interleukin-18 in cancer progression, Cancer Metastasis Rev. 25 (2006) 417−434.

[8] T. Ghayur, S. Banerjee, M. Hugunin, D. Butler, L. Herzog, A. Carter, et al., Caspase-1 processes IFN-gamma-inducing factor and regulates LPS-induced IFN-gamma production, Nature 386 (1997) 619−623.

[9] N. Tsutsumi, T. Kimura, K. Arita, M. Ariyoshi, H. Ohnishi, T. Yamamoto, et al., The structural basis for receptor recognition of human interleukin-18, Nat. Commun. 5 (2014) 5340.

[10] H. Ohnishi, H. Tochio, Z. Kato, N. Kawamoto, T. Kimura, K. Kubota, et al., TRAM is involved in IL-18 signaling and functions as a sorting adaptor for MyD88, PLoS One 7 (2012), e38423.

[11] S. Janssens, R. Beyaert, A universal role for MyD88 in TLR/IL-1R-mediated signaling, Trends Biochem. Sci. 27 (2002) 474−482.

[12] O. Adachi, T. Kawai, K. Takeda, M. Matsumoto, H. Tsutsui, M. Sakagami, et al., Targeted disruption of the MyD88 gene results in loss of IL-1- and IL-18-mediated function, Immunity 9 (1998) 143−150.

[13] J. Zhang, C. Ma, Y. Liu, G. Yang, Y. Jiang, C. Xu, Interleukin 18 accelerates the hepatic cell proliferation in rat liver regeneration after partial hepatectomy, Gene 537 (2014) 230−237.

[14] S. Matsumoto, K. Tsuji-Takayama, Y. Aizawa, K. Koide, M. Takeuchi, T. Ohta, et al., Interleukin-18 activates NF-kappaB in murine T helper type 1 cells, Biochem. Biophys. Res. Commun. 234 (1997) 454−457.

[15] H. Kojima, M. Takeuchi, T. Ohta, Y. Nishida, N. Arai, M. Ikeda, et al., Interleukin-18 activates the IRAK-TRAF6 pathway in mouse EL-4 cells, Biochem. Biophys. Res. Commun. 244 (1998) 183−186.

[16] H. Tsutsui, K. Matsui, N. Kawada, Y. Hyodo, N. Hayashi, H. Okamura, et al., IL-18 accounts for both TNF-alpha- and Fas ligand-mediated hepatotoxic pathways in endotoxin-induced liver injury in mice, J. Immunol. 159 (1997) 3961−3967.

[17] T. Hoshino, R.H. Wiltrout, H.A. Young, IL-18 is a potent coinducer of IL-13 in NK and T cells: a new potential role for IL-18 in modulating the immune response, J. Immunol. 162 (1999) 5070−5077.

[18] P. Bufler, T. Azam, F. Gamboni-Robertson, L.L. Reznikov, S. Kumar, C.A. Dinarello, et al., A complex of the IL-1 homologue IL-1F7b and IL-18-binding protein reduces IL-18 activity, Proc. Natl. Acad. Sci. U. S. A. 99 (2002) 13723−13728.

[19] M.F. Nold, C.A. Nold-Petry, J.A. Zepp, B.E. Palmer, P. Bufler, C.A. Dinarello, IL-37 is a fundamental inhibitor of innate immunity, Nat. Immunol. 11 (2010) 1014−1022.

[20] C.A. Nold-Petry, C.Y. Lo, I. Rudloff, K.D. Elgass, S. Li, M.P. Gantier, et al., IL-37 requires the receptors IL-18Ralpha and IL-1R8 (SIGIRR) to carry out its multifaceted anti-inflammatory program upon innate signal transduction, Nat. Immunol. 16 (2015) 354−365.

[21] D. Novick, S.H. Kim, G. Fantuzzi, L.L. Reznikov, C.A. Dinarello, M. Rubinstein, Interleukin-18 binding protein: a novel modulator of the Th1 cytokine response, Immunity 10 (1999) 127−136.

[22] T. Kunikata, K. Torigoe, S. Ushio, T. Okura, C. Ushio, H. Yamauchi, et al., Constitutive and induced IL-18 receptor expression by various peripheral blood cell subsets as determined by anti-hIL-18R monoclonal antibody, Cell. Immunol. 189 (1998) 135−143.

[23] D. Xu, W.L. Chan, B.P. Leung, D. Hunter, K. Schulz, R.W. Carter, et al., Selective expression and functions of interleukin 18 receptor on T helper (Th) type 1 but not Th2 cells, J. Exp. Med. 188 (1998) 1485−1492.

[24] R. Debets, J.C. Timans, T. Churakowa, S. Zurawski, R. de Waal Malefyt, K.W. Moore, et al., IL-18 receptors, their role in ligand binding and function: anti-IL-1RAcPL antibody, a potent antagonist of IL-18, J. Immunol. 165 (2000) 4950−4956.

[25] H. Persson, W. Ye, A. Wernimont, J.J. Adams, A. Koide, S. Koide, et al., CDR-H3 diversity is not required for antigen recognition by synthetic antibodies, J. Mol. Biol. 425 (2013) 803−811.

[26] F. Fellouse, S. Sidhu, Making Antibodies in Bacteria. Making and Using Antibodies, CRC Press, Boca Raton, FL, 2007.

[27] J.V. Weinstock, A. Blum, A. Metwali, D. Elliott, R. Arsenescu, IL-18 and IL-12 signal through the NF-kappa B pathway to induce NK-1R expression on T cells, J. Immunol. 170 (2003) 5003−5007.

[28] K. Konishi, F. Tanabe, M. Taniguchi, H. Yamauchi, T. Tanimoto, M. Ikeda, et al., A simple and sensitive bioassay for the detection of human interleukin-18/interferon-gamma-inducing factor using human myelomonocytic KG-1 cells, J. Immunol. Methods 209 (1997) 187−191.

[29] L.L. Reznikov, S.H. Kim, L. Zhou, P. Bufler, I. Goncharov, M. Tsang, et al., The combination of soluble IL-18Ralpha and IL-18Rbeta chains inhibits IL-18-induced IFN-gamma, J. Interferon Cytokine Res. 22 (2002) 593−601.

[30] T. Yoshimoto, K. Takeda, T. Tanaka, K. Ohkusu, S. Kashiwamura, H. Okamura, et al., IL-12 up-regulates IL-18 receptor expression on T cells, Th1 cells, and B cells: synergism with IL-18 for IFN-gamma production, J. Immunol. 161 (1998) 3400–3407.

[31] M. Bachmann, C. Dragoi, M.A. Poleganov, J. Pfeilschifter, H. Mühl, Interleukin-18 directly activates T-bet expression and function via p38 mitogen-activated protein kinase and nuclear factor-κB in acute myeloid leukemia–derived predendritic KG-1 cells, Mol. Cancer Ther. 6 (2007) 723–731.

[32] S.S. Rizk, J.L. Kouadio, A. Szymborska, E.M. Duguid, S. Mukherjee, J. Zheng, et al., Engineering synthetic antibody binders for allosteric inhibition of prolactin receptor signaling, Cell Commun. Signal. 13 (2015) 1.

[33] C.A. Nold-Petry, M.F. Nold, J.W. Nielsen, A. Bustamante, J.A. Zepp, K.A. Storm, J. Hong, S. Kim, C. Dinarello, Increased cytokine production in interleukin-18 receptor-deficient cells is associated with dysregulation of suppressors of cytokine signaling, J. Biol. Chem. 284 (2009) 25900–25911.

[34] X. Liu, M. Hammel, Y. He, J.A. Tainer, U.S. Jeng, L. Zhang, et al., Structural insights into the interaction of IL-33 with its receptors, Proc. Natl. Acad. Sci. U. S. A. 110 (2013) 14918–14923.

[35] G.P. Vigers, D.J. Dripps, C.K. Edwards 3rd, B.J. Brandhuber, X-ray crystal structure of a small antagonist peptide bound to interleukin-1 receptor type 1, J. Biol. Chem. 275 (2000) 36927–36933.

[36] B. Krumm, Y. Xiang, J. Deng, Structural biology of the IL-1 superfamily: key cytokines in the regulation of immune and inflammatory responses, Protein Sci. 23 (2014) 526–538.

[37] C. Thomas, J.F. Bazan, K.C. Garcia, Structure of the activating IL-1 receptor signaling complex, Nat. Struct. Mol. Biol. 19 (2012) 455–457.

[38] D. Wang, S. Zhang, L. Li, X. Liu, K. Mei, X. Wang, Structural insights into the assembly and activation of IL-1beta with its receptors, Nat. Immunol. 11 (2010) 905–911.

[39] A. Yamagata, T. Yoshida, Y. Sato, S. Goto-Ito, T. Uemura, A. Maeda, et al., Mechanisms of splicing-dependent trans-synaptic adhesion by PTPdelta-IL1RAPL1/IL-1RAcP for synaptic differentiation, Nat. Commun. 6 (2015) 6926.

[40] S. Kuruganti, S. Miersch, A. Deshpande, J.A. Speir, B.D. Harris, J.M. Schriewer, et al., Cytokine activation by antibody fragments targeted to cytokine-receptor signaling complexes, J. Biol. Chem. 291 (2016) 447–461.

[41] S.L. Barker, J. Pastor, D. Carranza, H. Quinones, C. Griffith, R. Goetz, et al., The demonstration of alphaKlotho deficiency in human chronic kidney disease with a novel synthetic antibody, Nephrol. Dial. Transplant. 30 (2015) 223–233.

[42] S. Moutel, A. El Marjou, O. Vielemeyer, C. Nizak, P. Benaroch, S. Duebel, et al., A multi-Fc-species system for recombinant antibody production, BMC Biotechnol. 9 (2009).

[43] S. Miersch, B.V. Maruthachalam, C.R. Geyer, S.S. Sidhu, Structure-directed and tailored diversity synthetic antibody libraries yield novel anti-EGFR antagonists, ACS Chem. Biol. 12 (2017) 1381–1389.

[44] F. Yi, S.S. Liu, F. Luo, X.H. Zhang, B.M. Li, Signaling mechanism underlying (2A)-adrenergic suppression of excitatory synaptic transmission in the medial prefrontal cortex of rats, Eur. J. Neurosci. 38 (2013) 2364–2373.

[45] T. Kimura, N. Tsutsumi, K. Arita, M. Ariyoshi, H. Ohnishi, N. Kondo, et al., Purification, crystallization and preliminary X-ray crystallographic analysis of human IL-18 and its extracellular complexes, Acta Crystallogr. F Struct. Biol. Commun. 70 (2014) 1351–1356.

[46] S. Trowitzsch, C. Bieniossek, Y. Nie, F. Garzoni, I. Berger, New baculovirus expression tools for recombinant protein complex production, J. Struct. Biol. 172 (2010) 45–54.

[47] W. Minor, M. Cymborowski, Z. Otwinowski, M. Chruszcz, HKL-3000: the integration of data reduction and structure solution–from diffraction images to an initial model in minutes, Acta Crystallogr. D Biol. Crystallogr. 62 (2006) 859–866.

[48] P.D. Adams, P.V. Afonine, G. Bunkoczi, V.B. Chen, I.W. Davis, N. Echols, et al., PHENIX: a comprehensive Python-based system for macromolecular structure solution, Acta Crystallogr. D Biol. Crystallogr. 66 (2010) 213–221.

[49] M. Biasini, S. Bienert, A. Waterhouse, K. Arnold, G. Studer, T. Schmidt, et al., SWISS-MODEL: modelling protein tertiary and quaternary structure using evolutionary information, Nucleic Acids Res. 42 (2014) W252–W258.

[50] P. Emsley, K. Cowtan, Coot: model-building tools for molecular graphics, Acta Crystallogr. D Biol. Crystallogr. 60 (2004) 2126–2132.

[51] E. Potterton, P. Briggs, M. Turkenburg, E. Dodson, A graphical user interface to the CCP4 program suite, Acta Crystallogr. D Biol. Crystallogr. 59 (2003) 1131–1137.

[52] R.A. Laskowski, M.W. MacArthur, D.S. Moss, J.M. Thornton, PROCHECK: a program to check the stereochemical quality of protein structures, J. Appl. Crystallogr. 26 (1993) 283–291.

[53] L. Holm, P. Rosenstrom, Dali server: conservation mapping in 3D, Nucleic Acids Res. 38 (2010) W545–W549.

[54] K.G. Tina, R. Bhadra, N. Srinivasan, PIC: protein interactions calculator, Nucleic Acids Res. 35 (2007) W473–W476.

[55] G.P. Poornam, A. Matsumoto, H. Ishida, S. Hayward, A method for the analysis of domain movements in large biomolecular complexes, Proteins 76 (2009) 201–212.

[56] M.P. Lefranc, C. Pommie, M. Ruiz, V. Giudicelli, E. Foulquier, L. Truong, et al., IMGT unique numbering for immunoglobulin and T cell receptor variable domains and Ig superfamily V-like domains, Dev. Comp. Immunol. 27 (2003) 55–77.